Topography of Hippocampal Connectivity with Sensorimotor Cortex Revealed by Optimizing Smoothing Kernel and Voxel Size

Douglas D. Burman[1]

[1]Department of Radiology, NorthShore University HealthSystem, 2650 Ridge Ave., Evanston, Illinois 60201, United States of America

Corresponding author:

Email: DBurman2@northshore.org (DB)

Abstract

Evaluating hippocampal connectivity across task conditions can be challenging, especially in the absence of activation to select the size and location of seeds; furthermore, optimal analysis parameters are unknown. Hippocampal task-specific connectivity with sensorimotor cortex was identified from psychophysiological interactions (PPI) during volitional movements; connectivity from a structural seed represented the mean of connectivity maps from all voxels in a hippocampal region, whereas connectivity from a functional seed represented maximal connectivity from an individual voxel. Motor activation and hippocampal connectivity were both evaluated across different processing parameters (3mm vs. 4mm isovoxels, smoothing kernels of 6-10mm). Topography in hippocampal connectivity was apparent along both its longitudinal axis and mediolateral axis, but only with optimal processing. Larger voxels improved signal-to-noise during individual and group analyses, lowering the statistical threshold and increasing the area of activation. The 10mm smoothing kernel was optimal for detecting connectivity from structural seeds, whereas the size of the smoothing kernel had little effect on connectivity from functional seeds. Unlike other approaches, structural seeds in this study allowed task-related connectivity to be examined throughout the hippocampus. By optimizing processing parameters, topography in hippocampal connectivity became demonstrable from both structural seeds and individual voxels. Larger voxels and smoothing kernels improved sensitivity for detecting activation and hippocampal connectivity, with the use of structural / functional seeds uncovering details about the topography of its functional connections.

Keywords: fMRI, connectivity, hippocampus, sensorimotor cortex, smoothing kernel, topography

Declarations of interest: none

1. Introduction

Connectivity analysis involves correlation of moment-by-moment changes in activity across brain regions; in functional magnetic resonance imaging (fMRI), this is represented by the blood oxygen-level dependent (BOLD) signal. Although temporal correlations need not depend on a task condition, task-dependent connectivity allows the study of brain interactions that underlie various motor, sensory, and cognitive abilities [1, 2]. Psychophysiological interactions (PPI) of the neural activity across tasks can be used to identify the task-specific influence of a seed region on other brain areas [3]. Seed selection can be critical in connectivity studies [4-6], yet because information carried in the temporal pattern of activity during a task is not necessarily accompanied by a mean change in activity, task activation is not necessary for seed selection. This is particularly relevant for the hippocampus, where the temporal pattern of its activity carries information [7-10].

Processing parameters can improve BOLD signal detection by reducing noise. Two fundamental considerations are voxel size and the size of the smoothing kernel [11]. Optimal voxel size should generally be commensurate with activation volume, although due to susceptibility field gradients, smaller voxel sizes may sometimes increase sensitivity despite less total signal intensity [12, 13]. Larger voxel sizes improve signal strength but provide lower spatial resolution, whereas hippocampal studies generally prefer better resolution due its small size; during analysis, voxel dimensions within any plane typically range from 1mm to 3mm [14-21].

Spatial smoothing increases signal-to-noise in BOLD signals and provides smoothness to imaged data [22, 23]. Smoothing expands the size of detected activation by reducing noise; generally, the optimal smoothing kernel is 2-3 times the voxel size, both for individual analysis [24, 25] and for large group analysis, although larger smoothing kernels are suggested for group analysis in

studies with fewer subjects [26]. Smoothing kernels may degrade the resolution of signal [27], so some studies of the hippocampus avoid smoothing [21], whereas others use a small Gaussian smoothing kernel ranging from 3-6mm full width at half maximum (FWHM) [16, 19, 28, 29]. Nonetheless, several hippocampal studies have used larger smoothing kernels of 8mm [14, 15, 18, 20, 30].

The selection of appropriate processing parameters raises challenges for connectivity studies, especially those designed to examine the influence of hippocampal activity on cortical areas that differ in optimal processing parameters. As it is for activation analysis, the optimal smoothing kernel for connectivity analysis is generally 2-3 times the voxel size [31]. With a few exceptions [32, 33], smoothing kernels used in hippocampal connectivity studies are small, ranging from 2-6mm [34, Heise, 2014 #6998, Menon, 2005 #6997].

The effects of voxel and smoothing kernel size in the hippocampus have not been explored empirically, so their precise relationship to activation and connectivity is unknown. Building on prior work [35], the current study systematically explores the effect of voxel size and smoothing kernel parameters on task-specific activation as well as PPI connectivity from hippocampus to sensorimotor cortex (SMC), evaluated from both multi-voxel structural seeds and single-voxel functional seeds. Results show modest effects of a larger voxel size on detecting activation (4mm vs. 3mm isovoxels); larger smoothing kernels improve sensitivity to hippocampal and SMC activation, and to hippocampal-SMC connectivity from structural seeds.

2. Materials and methods

2.1 Data availability

Subjects, task, data acquisition, and processing procedures have previously been described in detail [35, 36], with the dataset available for download [37].

2.2 Subjects

Thirteen normal right-handed adults participated in the following written consent study (ages 24-59, mean=42.3, five females); informed consent procedures complied with the Code of Ethics set forth in the Declaration of Helsinki, and were approved by the Institutional Review Board at the NorthShore University HealthSystem / Research Institute.

2.3 Experimental task

Each subject performed a visual/motor task, consisting of 6 cycles of a specified sequence of visual and motor conditions over a period of 6m 4s. Each cycle included a block of sequential tapping and a block of repetitive tapping, each separated by a passive visual condition. The task ended with 10s of passive fixation on a central cross.

During the sequential tapping block, a 4-button sequence to be remembered was displayed while a metronome ticked at 2 Hz; the subject pressed the remembered sequence of buttons in time with the metronome once the onscreen instructions were replaced with a cross. Subjects repeated the 4-button sequence throughout the 16s block, which ended when a circular checkerboard pattern flickered onscreen for 9s. During this visual block, subjects fixated the center of the pattern and refrained from moving.

During the repetitive tapping block, the subject was instructed to tap the same finger on both hands in synchrony with the metronome. Once the instruction screen was replaced with the number '1', the subject tapped the index finger from both hands; every 4s, the onscreen number

increased by one, and the subject changed finger. This motor condition was also followed by the passive visual condition.

Button presses were recorded from the right hand during both motor tasks to verify accurate performance. Behavioral analysis demonstrated motor learning and recall effects during the sequence learning task; anticipatory movements prior to the metronome demonstrated cognitive control of movements during both repetitive tapping and sequence learning [35].

2.4 MRI data acquisition

Images were acquired using a 12-channel head coil in a 3 Tesla Siemens scanner. BOLD functional images were acquired with echo planar imaging, using the following parameters: time of echo (TE) = 25 ms, flip angle = 90°, matrix size = 64 x 64, field of view = 22x22 cm, slice thickness = 3 mm, number of slices = 32; time of repetition (TR) = 2000 ms; and the number of repetitions = 182. These parameters produced in-plane voxel dimensions of 3.4 x 3.4mm. A structural T1 weighted 3D image (TR = 1600 ms, TE = 3.46 ms, flip angle = 9°, matrix size = 256 x 256, field of view = 22x22 cm, slice thickness = 1 mm, number of slices = 144) was acquired in the same orientation as the functional images.

2.5 fMRI data processing

Data were processed and analyzed using SPM12 software (http://www.fil.ion.ucl.ac.uk/spm). Images were spatially aligned to the first volume to correct for small movements. After removing one cycle from a subject's data set due to excessive head movements, maximal RMS movement for any subject was less than 1.5mm (mean = 0.850 $\pm$ 0.291mm). Sinc interpolation minimized timing-errors between slices; functional images were coregistered to the anatomical image, normalized to the standard T1 Montreal Neurological Institute (MNI) template, and

resliced for two sets of analyses. For one analysis, functional images were resliced as 3mm isovoxels, potentially improving in-plane image resolution by incorporating differences in signal intensity associated with small head movements. For the other analysis, functional images were resliced as 4mm isovoxels, thereby decreasing image resolution.

To identify task-related activation, copies of images from each dataset were smoothed with a 6mm, 8mm, or 10mm isotropic Gaussian kernel and filtered with a high pass cutoff frequency of 128s. Conditions of interest were specified for sequence learning, visual, and repetitive tapping, then modeled for block analysis using a canonical hemodynamic response function.

2.6 Activation analysis

A parameter estimate of the BOLD response to each condition was generated; motor activation was identified for each subject by contrasting mean BOLD responses to motor vs. passive visual conditions. Analyses used an intensity threshold of $p<0.05$ with a family-wise error (FWE) correction for multiple comparisons, applied to a sensorimotor region of interest (ROI). Typically, this ROI was specified as the overlap between TD and aal atlas labels for post- plus precentral gyrus in the WFUPickatlas toolbox for SPM. An additional analysis used the hand representation as the ROI [35] in order to evaluate whether effects of kernel size and smoothing kernel had a similar effect on activation parameters within the region known to be active.

For each voxel size and smoothing kernel combination, the mean and standard error of activation parameters from all individual subjects were recorded and quantitatively compared; these parameters included t-value threshold (corresponding to that required by the FWE correction), maxima t-values, and contrast amplitudes. Additionally, paired t-tests applied to individual

subject data allowed statistical comparison of different voxel sizes with each smoothing kernel, and between different smoothing kernels with the same voxel size.

For analysis of group effects, BOLD contrasts from individual subjects during the motor memory and repetitive tapping conditions were entered into a 1-sample t-test for each voxel size / smoothing kernel combination, recording the same parameters as noted above for individuals (t-threshold, maxima t-values, and contrast amplitudes). In addition, paired t-tests looked for significant group differences in activation between 6mm and 10mm smoothing kernels.

Differences in the size and location of activation from different conditions were identified visually from overlapping activation maps.

2.7 Connectivity analysis

2.7.1 Preprocessing

Psychophysiological interactions (PPI) were used to identify task-specific connectivity of the hippocampus with sensorimotor cortex [3, 38, 39]. Connectivity specific for finger movements was mapped for each hippocampal 4mm isovoxel (78 in the left and 78 in the right hippocampus of the normalized brain, as delimited by the aal atlas in the WFU PickAtlas toolbox for SPM). Multi-voxel structural seeds were defined by anatomical location. The hippocampus was divided into a 3x3 matrix, and a structural seed's connectivity map was calculated as the mean of connectivity maps from all voxels within the region. These structural seeds were labelled by their position within the matrix (A to C from anterior to posterior, 1 to 3 from medial to lateral) and sign of connectivity (positive or negative).

Connectivity from structural seeds guided analyses of connectivity from single voxels. For each structural seed that showed significant SMC connectivity, a connectivity map from a single voxel

was sampled; in addition, a functional seed was identified as the single voxel from the left and right hippocampus that showed maximal connectivity within the SMC mask. A functional seed was identified for both sequence learning ("memseed") and repetitive tapping ("tapseed"). Functional seeds reflected individual variability in functional localization, providing a better estimate of the magnitude and extent of hippocampal influence on SMC activity.

2.7.2 Group analysis

Beta estimates of connectivity from each subject's left and right hippocampus were entered into a two-cell ANOVA, using the hand representation delineated from activation analysis as the ROI and applying an intensity threshold of $p<0.05$ with FWE correction. This ROI provides optimal sensitivity for detecting effects, as hippocampal connectivity with SMC during volitional finger movements is selective for the hand representation [35].

3. Results

3.1 Effects of voxel size and smoothing kernels on SMC activation

As described in detail below, group and individual analyses showed similar trends of voxel size and smoothing kernels on patterns of SMC activation. During group analyses, differences in group activation between 3mm and 4mm isovoxels were small in magnitude, as were smoothing kernel effects *except* for activation volume. At the individual level, however, effects from different voxel sizes and smoothing kernels were both significant

For both 3mm and 4mm isovoxels, maxima values generally decreased incrementally with larger smoothing kernels. The maximal t-value decreased, a pattern observed during both group and individual analyses (Fig 1A); lower maxima t-values were observed during group analysis. Estimates for the magnitude of contrast effects also decreased, especially for individual analyses;

the magnitude of effects nearly converged for individual and group analyses for 10mm smoothing (see bottom of graphs). In addition, the threshold to identify significant activation dropped, resulting from less local variability in signal amplitude with increasing kernel size. During both individual and group analyses, the net effect was larger activation volumes with larger smoothing kernels, with 4mm isovoxels always generating larger activation volumes than 3mm isovoxels (Fig 1B). With a 10mm smoothing kernel, SMC activation from the two voxel sizes overlapped extensively, but with a slightly larger activation volume for 4mm isovoxels during sequence learning (Fig 1C).

Larger smoothing kernels thus provide greater sensitivity for detecting activation by reducing noise (random variability in signal). Comparing changes in activation volume with different ROIs provides further insight (Table 1). With the SMC mask, large increases in activation volume were observed as the smoothing kernel increased 6mm to 10mm, volume increases of 84.2 - 440.0%. These increases were much smaller within the hand representation, never exceeding 33.3% and nearly non-existent for 3mm isovoxels (volume increases of 1.9 – 1.6% for repetitive tapping and sequence learning, respectively). This suggests larger smoothing kernels are particularly effective for improving statistical detection by reducing signal variability outside the activated region, thus requiring a smaller mean difference in signal to detect activation.

Because data from the same individuals were processed with different voxel size and smoothing kernels, the magnitude of differences in activation parameters for each individual could be statistically compared for different processing parameters. Although the standard error across the group often differed substantially, paired t-tests revealed that individuals consistently had lower activation thresholds and greater activation volumes with larger (4mm) isovoxels, regardless of smoothing kernel (Table 2).

For each task, the effects of different smoothing kernels on activation parameters were also evaluated with paired t-tests (Tables 3-4). With 3mm isovoxels, larger smoothing kernels during both motor tasks generated higher activation volumes, but significantly lower maxima t-values, contrast magnitudes, and activation thresholds. These same patterns were generally observed with 4mm isovoxels, except no differences between 8mm and 10mm smoothing kernels were observed for threshold or contrast magnitude during repetitive tapping (Table 3), or for maxima t-values and contrast magnitudes during sequence learning (Table 4).

To summarize, 4mm isovoxels provided greater sensitivity to activation than 3mm isovoxels (lower threshold and higher activation volume), as did 10mm compared with 6mm smoothing kernels (for both 3mm and 4mm isovoxels). For 4mm isovoxels, differences between 8mm and 10mm smoothing kernels were less differentiated for some activation parameters.

3.2 Effect of smoothing kernels on hippocampal motor activation

Using the hippocampal ROI mask, group analysis failed to demonstrate motor activation for any combination of voxel size and smoothing kernel. Using paired t-tests to compare activation following 10mm vs. 6mm smoothing, however, more intense activation was observed from the larger smoothing kernel during both motor tasks (Figs 2-3). For both 3mm and 4mm isovoxels, the most intense activation (orange) was observed along the border between structural seeds B1 and C1; mildly elevated activation (yellow) was observed throughout B1.

3.3 Hippocampal connectivity: Structural seeds

Connectivity from a structural seed represented the mean of connectivity maps from each voxel within the region. Negative connectivity was observed from many structural seeds (Table 5). With smoothing kernels of 6mm and 10mm, structural seeds often showed similar maxima

locations in the pre- and postcentral gyri; the volume of connectivity, however, was invariably greater with the larger smoothing kernel.

Small differences in location within SMC were observed for connectivity from different smoothing kernels. For the repetitive tapping task, a topographic arrangement of connectivity based upon seed location was discernible, depending on the size of the smoothing kernel (Fig 4). For the long (anterior / posterior) axis of the hippocampus, the organization was apparent among medial seeds with the 10mm smoothing kernel (Fig 4A, right). Connectivity for each of these seeds was centered in the precentral gyrus, barely extending across the central sulcus into the postcentral gyrus. From the anterior hippocampal seed A1 (red), intense connectivity projected further anterolateral; the middle seed B1 projected superomedial (yellow), whereas the posterior seed C1 projected further medial and posterior (green). Because its clusters were smaller and spotty, this topography was indiscernible with the 6mm smoothing kernel (Fig 4A, left).

By contrast, a topographic organization in structural seed connectivity was better suggested along the medial / lateral axis of the hippocampus with the 6mm smoothing kernel (Fig 4B left); connectivity from more lateral seeds extended further posterior. This topography was less apparent with 10mm smoothing (Fig 4B, right), because larger clusters of connectivity produced extensive overlap.

However, topography is demonstrable from individual voxels with 10mm smoothing along both the medial-lateral and longitudinal axes (Fig 5). In the medial-lateral plane, the organization is seen in the pattern of overlapping connectivity maps (Fig 5A, left), and by using differential connectivity maps to illustrate which seeds generated the greatest amplitude of connectivity (Fig 5A, right). Along the longitudinal axis, topography was readily observable, with little overlap

from individual voxels (Fig 5B). For all these voxels, connectivity included both pre- and postcentral gyrus, although precentral connectivity was more extensive during repetitive tapping; during sequential learning, connectivity was more extensive in the postcentral gyrus of the left hemisphere (Table 6).

Overall, the 10mm smoothing kernel provided better sensitivity for structural seeds to demonstrate both hippocampal connectivity and topography.

3.4 Hippocampal connectivity: Functional seeds

Functional seeds showed unilateral connectivity during group analysis. Tapseed^{-} generated right-hemispheric connectivity during the repetitive tapping task (Fig 6A, red), whereas memseed^{-} generated connectivity in the left hemisphere (Fig 6A, yellow). Smoothing kernels of 6mm and 10mm showed little or no difference in connectivity from tapseed^{-} during repetitive tapping or from memseed^{-} during sequence learning; the extent of connectivity was, however, larger with the 10mm kernel for memseed^{+} during sequence learning (see Table 5).

The 10mm smoothing kernel increased the intensity of connectivity as well as its extent. As noted earlier, a few hippocampal voxels individually show greater activation with a 10mm vs. 6mm smoothing kernel; these same voxels generated greater intensity of connectivity (orange), interspersed within the area of connectivity shown by functional seeds in both tasks (Fig 6B).

4. Discussion

This study evaluated the effect of voxel size (3mm vs. 4mm isovoxels) and smoothing kernels (6-10mm) on motor activation and hippocampal connectivity with SMC; connectivity analyses included both multi-voxel structural seeds and single-voxel functional seeds, the latter selected to

account for individual variability in functional localization. Larger voxels modestly improved sensitivity for detecting activation in SMC; contrary to expectations, larger smoothing kernels also improved sensitivity for detecting both hippocampal activation and connectivity from multi-voxel structural seeds. Kernel effects were smaller for functional seeds; for single voxels at specified anatomical locations, however, sensitivity adequate to map the topography of hippocampal connectivity required larger smoothing kernels.

4.1 Effects of voxel size and smoothing kernel on cortical activation

In this study, voxel size had modest effects on activation. In SMC, larger voxels (4mm) showed a smaller statistical threshold and a larger activation volume during both repetitive tapping and sequence learning, but these effects were small, requiring direct within-subject comparisons via paired t-tests to demonstrate. Group comparisons of the mean showed no effect of voxel size, and visual comparison of random-effects activation showed only minor differences in the area of activation along cluster borders, mostly seen during sequence learning. Furthermore, no significant differences in contrast magnitude were observed between 3mm and 4mm isovoxels, regardless of smoothing kernel. Although the larger 4mm isovoxels provide slightly better sensitivity for detecting cortical activation, this effect was modest.

The effect of smoothing kernel on *cortical* activation depended on the ROI. With the SMC mask, increases in the smoothing kernel from 6mm to 10mm resulted in the detection of much greater activation volumes; within the hand representation, this increase in activation volume was much less. This suggests the larger smoothing kernel more effectively reduced random variability (noise) in inactive regions within the SMC mask, reducing the mean difference in

signal required to detect activation. This interpretation is consistent with observed decreases in the maxima t-value, contrast magnitude, and threshold.

During both individual and group analysis, the largest (10mm) smoothing kernel applied to 4mm isovoxels was most sensitive for detecting activation. This was not simply an overestimation of activation size from a large smoothing kernel [24]; global analysis across both tasks demonstrated an even larger, bilateral area of activation consistent with task behavior [35]. With these processing parameters, the contrast estimate at the maxima from group analysis approached the mean value from individual analyses, suggesting this combination of voxel size and smoothing kernel provided the most accurate group representation of sensorimotor activation.

4.2 Effect of smoothing kernel on hippocampal activation

Using conventional group analysis, the hippocampus did not show motor activation during repetitive movements or sequence learning. By using paired t-tests to compare motor activation across different smoothing kernels, greater activation was demonstrated using the 10mm vs. 6mm smoothing kernel, evident with both 3mm and 4mm isovoxels. This differential activation occurred in the medial hippocampus, mostly within the central third of the hippocampus but extending slightly into the posterior third, most intense at the boundary between the B1 (central-medial) and C1 (posterior-medial) structural seeds.

During smoothing, local variability is minimized by recalculating the BOLD signal based upon peaks and their surrounding signal, fit to a Gaussian curve. When activity surrounding a 4mm isovoxel showing peak activity is symmetrical, both a 6mm and 10mm smoothing kernel utilize the magnitude of signal from a single voxel on each side in its calculation, differing only in the weighting provided from the adjacent voxel (3mm on each side of the peak 4mm-voxel using a

10mm kernel, and 1mm on each side of the peak 4mm-voxel with a 6mm kernel). Activity surrounding a peak voxel near the edge of gray matter is asymmetrical; the calculated peak coordinate is shifted toward the higher activity within gray matter, away from the edge [40, 41]. Thus, differential activation from the larger smoothing kernel did not result from extending the smoothed signal outside hippocampal boundaries; instead, the 10mm kernel provided a better estimate of local activation by more fully incorporating information from nearby activity.

The region showing differential activation showed more intense and widespread SMC connectivity following 10mm smoothing. Thus, improved sensitivity for detecting local hippocampal activity with the larger smoothing kernel also improved sensitivity for detecting regional connectivity.

4.3 Effect of smoothing kernel on hippocampal connectivity

Direct comparisons between different smoothing kernels showed no significant difference in the amplitude of connectivity from structural seeds. Although the amplitude of peak connectivity was typically lower (as measured by t-value), structural seeds demonstrated larger clusters of SMC connectivity with the larger kernel in both motor tasks. A connectivity map from a structural seed represents the mean connectivity from every voxel within the designated region of hippocampus, so larger connectivity clusters reflect the effectiveness of the smoothing kernel in reflecting local regional activity (see also [42]).

With the 6mm smoothing kernel, a topographic pattern from structural seeds was evident along the medial-lateral axis of the hippocampus, but not the longitudinal axis, which generated small and disparate clusters with no apparent topography. With the 10mm kernel, a topographic pattern from structural seeds was evident along the longitudinal axis of the hippocampus, but not

the medial-lateral axis, due to extensive overlap in connectivity from adjacent seeds. With the 10mm kernel, a topographic pattern was nonetheless evident from the connectivity of individual voxels along either axis.

The size of the smoothing kernel may be a factor in detecting functional heterogeneity within the hippocampus. A resting state connectivity study using a small (3mm) smoothing kernel failed to find functional heterogeneity along the anterior-posterior axis [43], whereas a study of connectivity from the hippocampus to cortical regions during episodic memory found functional heterogeneity along the same axis using a larger (5mm) smoothing kernel [34].

In summary, the 10mm smoothing kernel was advantageous for demonstrating hippocampal topography in its connectivity with SMC, both for structural seeds and individual voxels at specified locations.

4.4 Topography of hippocampal connectivity

Similar to previous studies, hippocampal connectivity in this study showed a topographical organization along both the long anterior-posterior axis [44-47] and medial-lateral axis [44].

In the current study, hippocampal connectivity with SMC was preferentially seen within the SMC hand representation, with location and laterality similar to group activation for both tasks. Except for right-hemisphere connectivity from memseed^{+}, activation and connectivity were both observed in the left SMC during sequence learning (reflecting right-handed movements) and the right SMC during repetitive tapping (despite bilateral hand movements). Furthermore, activation and connectivity both covered the breadth of the postcentral gyrus within the hand representation during sequence learning, whereas activation and connectivity were centered in precentral gyrus

during repetitive tapping (with postcentral effects adjacent to the central sulcus). Whether these task differences arose from differences in behavioral requirements, hand dominance (right-handed subjects), or hemispheric differences in motor function is unknown.

The role of hippocampal topography to SMC function is unclear. Within the hand area of the precentral gyrus, overlapping but distinguishable regions are involved in wrist and individual finger movements [48-51], whereas multiple representations for each digit may differentially reflect flexion and extension movements [52], or different degrees of movement complexity [53]. Similarly, somatotopy for individual fingers in postcentral gyrus are overlapping but distinguishable, with multiple representations across the anterior-posterior width of the gyrus [54-56]. Methods here did not allow mapping onto individual finger representations, or even flexion vs. extension, so the functional significance of the hippocampal topography is currently unclear.

Different cognitive functions have been suggested for anterior vs. posterior hippocampus. Suggested differences in function include encoding vs. recall [57, 58], internal vs. external attention [59], gist/conceptual vs. detailed/spatial information [60-62], and pattern completion vs. separation [63]. In the current study, the topographical pattern of connectivity observed from anterior vs. posterior hippocampus is inconsistent with these roles, particularly as the repetitive tapping task required paced, volitional movements without learning or memory recall[35]. Topographical connectivity with different regions within the pre- or postcentral hand representation suggest a role more directly involved in motor control, perhaps coordinating cognitive and motor functions to facilitate and suppress muscle actions required for the correct timing of finger movements [36, 51].

4.5 Practical considerations for future studies

Many hippocampal studies have used small voxels and smoothing kernels, believing these processing parameters provide data that more accurately reflect true hippocampal activity. The current study suggests otherwise, particularly when examining hippocampal connectivity with cortical areas.

Paired t-tests comparing cortical activation with 4mm vs. 3mm isovoxels showed lower thresholds and larger volumes of activation from larger voxels, with additional volume along the edges of an activation cluster. Similarly, larger smoothing kernels decreased the threshold and increased the volume of cortical activation. During sequence learning, even small differences in activation between 8mm and 10mm smoothing kernels were significant, although differences between 8mm and 10mm smoothing kernels were not significant for 4mm isovoxels during repetitive tapping. These findings indicate that 4mm isovoxels with 8-10mm smoothing kernels are more sensitive for detecting cortical activation.

Larger smoothing kernels also improved the signal-to-noise ratio associated with local hippocampal activity. Although group analysis failed to detect movement-related activation, direct comparison demonstrated greater activation in localized areas of the hippocampus activation with 10mm vs. 6mm smoothing kernels. These hippocampal areas also showed elevated connectivity with SMC, indicating this activation was functionally relevant.

For structural seeds, improved sensitivity with the 10mm smoothing kernel helped identify a topographic organization that was indiscernible with the 6mm smoothing kernel. The sensitivity of functional seeds was less affected by the size of the smoothing kernel, perhaps by accounting

for individual variability in localized function. In other brain areas, such individual variability in localized function has been correlated with age and cognitive abilities [64].

Although effects from smaller smoothing kernels may be mitigated by accounting for individual variability in functional localization, results from this study suggest larger voxels and smoothing kernels can provide better study outcomes for hippocampal connectivity studies. Results also illustrate advantages of the structural / functional seed approach to examine hippocampal connectivity, particularly when functional localization is unknown from its activation. By calculating connectivity from each voxel, results did not depend on ideal selection of seed location or size; topographic differences in projection were serendipitously identified here by averaging connectivity maps from different regions.

5. Conclusions

Processing fMRI data with a larger voxel size (4mm) and smoothing kernel (8-10mm) can improve sensitivity to hippocampal activity and its connectivity with cortical areas; in this study, optimizing these processing parameters uncovered topography in hippocampal connectivity along two axes. Lesser sensitivity when using a smaller smoothing kernel may be offset in some analyses by using small seeds that take into account individual variability in functional localization.

6. Acknowledgments

The author wishes to thank the Center for Advanced Imaging (CAI) at NorthShore University HealthSystem for its administrative support.

Funding: This research did not receive any specific grant from funding agencies in the public, commercial, or not-for-profit sectors.

7. References

1. Friston KJ. Functional and effective connectivity: A review. Brain Connectivity. 2011;1(1):13-36.

2. Li K, Guo L, Nie J, Li G, Liu T. Review of methods for functional brain connectivity detection using fMRI. Computerized Medical Imaging and Graphics. 2009;2(33):131-9.

3. O'Reilly JX, Woolrich MW, Behrens TEJ, Smith SM, Johansen-Berg H. Tools of the trade: Psychophysiological interactions and functional connectivity. Social Cognitive and Affective Neuroscience. 2012;7(5):604-9.

4. Liu X, Zhu X-H, Qiu P, Chen W. A correlation-matrix-based hierarchical clustering method for functional connectivity analysis. Journal of Neuroscience Methods. 2012;211(1):94-102.

5. Ma L, Wang B, Chen X, Xiong J. Detecting functional connectivity in the resting brain: a comparison between ICA and CCA. Magnetic Resonance Imaging. 2007;25(1):47-56.

6. Sohn WS, Yoo K, Lee Y-B, Seo SW, Na DL, Jeong Y. Influence of ROI selection on resting state functional connectivity: an individualized approach for resting state fMRI analysis. Frontiers in Neuroscience. 2015.

7. Dan Y, Poo M-M. Spike timing-dependent plasticity: From synapse to perception. Physiological Reviews 2006;86(3):1033-48.

8. Hsieh L-T, Gruber MJ, Jenkins LJ, Ranganath C. Hippocampal activity patterns carry information about objects in temporal context. Neuron. 2014;81(5):1165-78.

9. Klausberger T, Somogyi P. Neuronal Diversity and Temporal Dynamics: The Unity of Hippocampal Circuit Operations. Science. 2008:53-7.

10. MacDonald CJ, Lepage KQ, Eden UT, Eichenbaum H. Hippocampal "time cells" bridge the gap in memory for discontiguous events. Neuron. 2011;71(4):737-49.

11. Hopfinger JB, Büchel C, Holmes AP, Friston KJ. A study of analysis parameters that influence the sensitivity of event-related fMRI analyses. NeuroImage. 2000;11(4):326-33.

12. Chen N-K, Dickey CC, Yoo S-S, Guttmann CRG, Panych LP. Selection of voxel size and slice orientation for fMRI in the presence of susceptibility field gradients: application to imaging of the amygdala. NeuroImage. 2003;19(3):817-25.

13. Thulborn KR, Chang SY, Shen GX, Voyvodic JT. High-resolution echo-planar fMRI of human visual cortex at 3.0 tesla. NMR in Biomedicine. 1997;10(4-5):183-90.

14. Danker JF, Tompary A, Davachi L. Trial-by-trial hippocampal encoding activation predicts the fidelity of cortical reinstatement during subsequent retrieval. Cerebral Cortex. 2017;27(7):3515-24.

15. Forcato C, Bavassi L, De Pino G, Fernández RS, Villarreal MF, Pedreira ME. Differential left hippocampal activation during retrieval with different types of reminders: An fMRI study of the reconsolidation process. PLoS One. 2016;11(3):e0151381.

16. Lech RK, Suchan B. Involvement of the human medial temporal lobe in a visual discrimination task. Behavioural Brain Research. 2014;268:22-30.

17. Liu Z-X, Shen K, Olsen RK, Ryan JD. Visual sampling predicts hippocampal activity. Journal of Neuroscience. 2017;37(3):599-609.

18. Mayes AR, Montaldi D, Roper A, Migo EM, Gholipour T, Kafkas A. Amount, not strength of recollection, drives hippocampal activity: A problem for apparent word familiarity-related hippocampal activation. Hippocampus. 2019;29(1):46.

19. Qin S, Cho S, Chen T, Rosenberg-Lee M, Geary DC, Menon V. Hippocampal-neocortical functional reorganization underlies children's cognitive development. Nature Neuroscience. 2014;17(9):1263-9.

20. Sperling R, Chua E, Cocchiarella A, Rand-Giovannetti E, Poldrack R, Schacter DL, et al. Putting names to faces: Successful encoding of associative memories activates the anterior hippocampal formation. NeuroImage. 2003;20(2):1400-10.

21. Zeidman P, Lutti A, Maguire EA. Investigating the functions of subregions within anterior hippocampus. Cortex. 2015;73:240-56.

22. Acton PD, Friston KJ. Statistical parametric mapping in functional neuroimaging: beyond PET and fMRI activation studies. Eur J Nucl Med. 1998;(25):663-7.

23. Worsley KJ. Spatial smoothing of autocorrelations to control the degrees of freedom in fMRI analysis. NeuroImage. 2005;26:635-41.

24. Liu P, Calhoun V, Chen Z. Functional overestimation due to spatial smoothing of fMRI data. Journal of Neuroscience Methods. 2017;291:1.

25. Pajula J, Tohka J. Effects of spatial smoothing on inter-subject correlation based analysis of FMRI. Magnetic Resonance Imaging. 2014;32(9):1114-24.

26. Mikl M, Marecek R, Hlustík P, Pavlicová M, Drastich A, Chlebus P, et al. Effects of spatial smoothing on fMRI group inferences. Magnetic resonance imaging. 2008;26(4):490-503.

27. Murphy JE, Yanes JA, Kirby LAJ, Reid MA, Robinson JL. Left, right, or bilateral amygdala activation? How effects of smoothing and motion correction on ultra-high field, high-resolution functional magnetic resonance imaging (fMRI) data alter inferences. Neuroscience Research. 2020;150:51-9.

28. Adcock RA, Thangavel A, Whitfield-Gabrieli S, Knutson B, Gabrieli JDE. Reward-motivated learning: Mesolimbic activation precedes memory formation. Neuron. 2006;50(3):507-17.

29. Selmeczy D, Fandakova Y, Grimm KJ, Bunge SA, Ghetti S. Longitudinal trajectories of hippocampal and prefrontal contributions to episodic retrieval: Effects of age and puberty. Developmental Cognitive Neuroscience. 2019;36:100599-611.

30. Rigoli F, Michely J, Friston KJ, Dolan RJ. The role of the hippocampus in weighting expectations during inference under uncertainty. Cortex. 2019;115:1-14.

31. Chen Z, Calhoun V. Effect of spatial smoothing on task fMRI ICA and functional connectivity. Frontiers in Neuroscience. 2018;12:15. PubMed PMID: https://doi.org/10.3389/fnins.2018.00015.

32. Smith APR, Stephan KE, Rugg MD, Dolan RJ. Task and content modulate amygdala-hippocampal connectivity in emotional retrieval. Neuron. 2006;4(49):631-8.

33. Wang L, LaViolette P, O'Keefe K, Putcha D, Bakkour A, Van Dijk KRA, et al. Intrinsic connectivity between the hippocampus and posteromedial cortex predicts memory performance in cognitively intact older individuals. NeuroImage. 2010;2(51):910-7.

34. Geng F, Redcay E, Riggins T. The influence of age and performance on hippocampal function and the encoding of contextual information in early childhood. NeuroImage. 2019;195:433-43.

35. Burman DD. Hippocampal connectivity with sensorimotor cortex during volitional finger movements: Laterality and relationship to motor learning. PloS One. 2019;14(9):e0222064.

36. Burman DD. Hippocampal connectivity with sensorimotor cortex during volitional finger movements. II. Spatial and temporal selectivity. bioRxiv. 2018;doi: https://doi.org/10.1101/479436.

37. Burman DD. Functional MRI dataset during passive visual stimulation and two motor conditions (sequence learning, paced repetitive tapping). NITRC. 2019. PubMed PMID: 10.25790/bml0cm.53.

38. Friston KJ, Buechel C, Fink GR, Morris J, Rolls E, Dolan RJ. Psychophysiological and modulatory interactions in neuroimaging. NeuroImage. 1997;6(3):218-29.

39. Gitelman DR, Penny WD, Ashburner J, Friston KJ. Modeling regional and psychophysiologic interactions in fMRI: The importance of hemodynamic deconvolution. NeuroImage. 2003;19(1):200-7.

40. Jo HJ, Lee J-M, Kim J-H, Choi C-H, Gu B-M, Kang D-H, et al. Artificial shifting of fMRI activation localized by volume- and surface-based analyses. NeuroImage. 2008;40(3):1077-89.

41. Sacchet MD, Knutson B. Spatial smoothing systematically biases the localization of reward-related brain activity. NeuroImage. 2013;66:270-7.

42. Wu CW, Chen C-L, Liu P-Y, Chao Y-P, Biswal BB, Lin C-P. Empirical evaluations of slice-timing, smoothing, and normalization effects in seed-based, resting-state functional magnetic resonance imaging analyses. Brain Connectivity. 2011;1(5):401-10.

43. Wang S-F, Ritchey M, Libby LA, Ranganath C. Functional connectivity based parcellation of the human medial temporal lobe. Neurobiology of Learning and Memory. 2016;(134):123-34.

44. de Wael RV, Larivière S, Caldairou Bt, Hong S-J, Margulies DS, Jefferies E, et al. Anatomical and microstructural determinants of hippocampal subfield functional connectome embedding. Proceedings of the National Academy of Sciences of the United States of America. 2018;115(40):10154.

45. Qin S, Duan X, Supekar K, Chen H, Chen T, Menon V. Large-scale intrinsic functional network organization along the long axis of the human medial temporal lobe. Brain Structure and Function. 2016;221(6):3237-58.

46. Robinson JL, Barron DS, Kirby LAJ, Bottenhorn KL, Hill AC, Murphy JE, et al. Neurofunctional topography of the human hippocampus. Human Brain Mapping. 2015;36(12):5018-37.

47. Strange BA, Witter MP, Lein ES, Moser EI. Functional organization of the hippocampal longitudinal axis. Nature Reviews Neuroscience. 2014;15(10):655.

48. Beisteiner R, Windischberger C, Lanzenberger R, Edward V, Cunnington R, Erdler M, et al. Finger somatotopy in human motor cortex.[see comment]. NeuroImage. 2001;13(6 Pt 1):1016-26.

49. Burman DD, Lie-Nemeth T, Brandfonbrener AG, Parisi T, Meyer JR. Altered Finger Representations in sensorimotor cortex of musicians with focal dystonia: Precentral cortex. Brain Imaging and Behavior. 2009;3(1):10-23.

50. Kleinschmidt A, Nitschke MF, Frahm J. Somatotopy in the human motor cortex hand area. A high-resolution functional MRI study. European Journal of Neuroscience. 1997;9(10):2178-86.

51. Sanes JN, Donoghue JP, Thangaraj V, Edelman RR, Warach S. Shared neural substrates controlling hand movements in human motor cortex. Science. 1995;268(5218):1775-8.

52. Zartl M, Kapfer T, Muellbacher W. Functional topography of cortical thumb movement representations in human primary motor cortex. Brain Topography. 2014;27(2):228-39.

53. Lotze M, Erb M, Flor H, Huelsmann E, Godde B, Grodd W. fMRI evaluation of somatotopic representation in human primary motor cortex. NeuroImage. 2000;11(5 Pt 1):473-81.

54. Blankenburg F, Ruben J, Meyer R, Schwiemann J, Villringer A. Evidence for a rostral-to-caudal somatotopic organization in human primary somatosensory cortex with mirror-reversal in areas 3b and 1. Cerebral Cortex. 2003;13(9):987-93.

55. Kurth R, Villringer K, Mackert BM, Schwiemann J, Braun J, Curio G, et al. fMRI assessment of somatotopy in human Brodmann area 3b by electrical finger stimulation. NeuroReport. 1998;9(2):207-12.

56. van Westen D, Fransson P, Olsrud J, Rosen B, Lundborg G, Larsson EM. Finger somatotopy in area 3b: an fMRI-study. BMC Neuroscience. 2004;5:28.

57. Lepage M, Habib R, Tulving E. Hippocampal PET activations of memory encoding and retrieval: the HIPER model. Hippocampus. 1998;8(4):313-22.

58. Rombouts SA, Barkhof F, Witter MP, Machielsen WC, Scheltens P. Anterior medial temporal lobe activation during attempted retrieval of encoded visuospatial scenes: an event-related fMRI study. NeuroImage. 2001;14(1 Pt 1):67-76.

59. Kim H. Encoding and retrieval along the long axis of the hippocampus and their relationships with dorsal attention and default mode networks: the HERNET model. Hippocampus. 2015;25(4):500-10.

60. Brunec IK, Bellana B, Ozubko JD, Man V, Robin J, Liu Z-X, et al. Multiple scales of representation along the hippocampal anteroposterior axis in humans. Current Biology. 2018;28(13):2129-35. e6.

61. Nadel L, Hoscheidt S, Ryan LR. Spatial cognition and the hippocampus: the anterior-posterior axis. Journal of Cognitive Neuroscience. 2013;25(1):22-8.

62. Sheldon S, McAndrews MP, Pruessner J, Moscovitch M. Dissociating patterns of anterior and posterior hippocampal activity and connectivity during distinct forms of category fluency. Neuropsychologia. 2016;90:148-58.

63. Poppenk J, Evensmoen HR, Moscovitch M, Nadel L. Long-axis specialization of the human hippocampus. Trends in Cognitive Sciences. 2013;17(5):230-40.

64. Burman DD, Minas T, Bolger DJ, Booth JR. Age, sex, and verbal abilities affect location of linguistic connectivity in ventral visual pathway. Brain and Language. 2013;124(2):184-93.

Table 1. Effect of voxel size and smoothing kernel on sensorimotor cortical activation from random effects group analysis during motor tasks.

Repetitive tapping	**Sensorimotor cortex**				**Hand representation**		
3mm isovoxels	coordinates	t-value	extent	volume	coordinates	extent	volume
smooth 0	(39,-22,59)	7.97	6	162	(39,-22,59)	25	675
smooth 6	(33,-16,59)	7.67	31	837	(33,-16,59)	108	2916
smooth 8	(33,-16,59)	7.15	60	1620	(33,-16,59)	110	2970
smooth 10	(33,-16,56)	6.49	83	2241	(33,-16,56)	110	2970
4mm isovoxels							
smooth 0	(42,-16,50)	6.36	4	256	(42,-16,50)	11	704
smooth 6	(34,-16,58)	6.73	19	1216	(34,-16,58)	47	3008
smooth 8	(34,-16,58)	6.57	32	2048	(34,-16,58)	50	3200
smooth 10	(34,-16,58)	6.05	35	2240	(34,-16,58)	53	3392
Sequence learning							
3mm isovoxels	coordinates	t-value	extent	volume	coordinates	extent	volume
smooth 0	(-36,-13,59)	7.71	1	27	(-36,-13,59)	1	27
smooth 6	(-42,-37,53)	7.05	4	108	(-39,-40,47)	61	1647
smooth 8	(-42,-37,53)	6.79	12	324	(-37,-37,47)	62	1674
smooth 10	(-39,-37,50)	6.62	35	945	(-37,-37,47)	62	1674
4mm isovoxels							
smooth 0	--	--	0	0	(-38,-16,54)	3	192
smooth 6	(-42,-36,54)	7.07	5	320	(-42,-36,54)	60	3840
smooth 8	(-42,-36,54)	6.76	11	704	(-42,-36,54)	77	4928
smooth 10	(-38,-36,50)	6.23	27	1728	(-38,-36,50)	80	5120

Region-of-interest (ROI) activation met an intensity threshold of p=0.05 with a family-wise error (FWE) correction. The sensorimotor ROI represented the pre/postcentral gyrus overlap between the aal and talairach atlases, as designated in the WFU PickAtlas toolbox for SPM; the hand representation was that used in a previous report (Burman, 2019). Coordinates and t-values represent activation maxima.

Table 2. Effects of voxel size on SMC activation.

maxima t-value	**Repetitive tapping**			
	0mm	6mm	8mm	10mm
mean difference[†]	-0.549±0.371	-0.322±0.495	-0.523±0.238	-0.319±0.263
p-value	0.165	0.529	0.048*	0.250
contrast magnitude				
mean difference	-0.618±0.322	-0.106±0.105	-0.192±0.115	-0.116±0.095
p-value	0.079	0.334	0.121	0.245
threshold t-value				
mean difference	-0.217±0.001	-0.124±0.001	-0.171±0.050	-0.127±0.003
p-value	<0.001*	<0.001*	<0.001*	<0.001*
activation volume				
mean difference	213.1±302.1	732.5±196.8	642.9±275.6	421.1±306.7
p-value	0.002*	0.003*	0.003*	0.004*
maxima t-value	**Sequence learning**			
	0mm	6mm	8mm	10mm
mean difference	-0.908±0.342	-0.509±0.347	-0.410±0.193	0.517±0.339
p-value	0.021*	0.168	0.056	0.154
contrast magnitude				
mean difference	0.143±0.381	0.169±0.346	0.314±0.233	-0.165±0.165
p-value	0.714	0.635	0.204	0.338
threshold t-value				
mean difference	-0.217±0.001	-0.124±0.001	-0.122±0.002	-0.127±0.003
p-value	<0.001*	<0.001*	<0.001*	<0.001*
activation volume				
mean difference	635.3±192.8	609.2±353.6	327.2±450.4	532.0±507.4
p-value	0.001*	0.001*	<0.001*	<0.001*

[†] At each smoothing kernel, differences in value were calculated for each individual from subject data resliced with 3mm vs. 4mm isovoxels; the mean difference ± standard error is listed.

* $p<0.05$ in a paired t-test.

Table 3. Smoothing kernel effects on SMC activation during repetitive tapping.

maxima t-value	**3mm isovoxels**			
	0mm	6mm	8mm	10mm
group mean	*12.64±1.34*	*11.89±1.36*	*11.13±1.35*	*10.30±1.27*
0mm	NA	0.075	0.004*	<0.001*
6mm	--	NA	<0.001*	<0.001*
8mm	--	--	NA	<0.001*
contrast magnitude				
group mean	*3.16±0.34*	*1.80±0.21*	*1.57±0.23*	*1.31±0.19*
0mm	NA	<0.001*	<0.001*	<0.001*
6mm	--	NA	<0.001*	<0.001*
8mm	--	--	NA	<0.001*
threshold t-value				
group mean	*4.24±0.01*	*4.01±0.02*	*3.87±0.02*	*3.77±0.02*
0mm	NA	<0.001*	<0.001*	<0.001*
6mm	--	NA	<0.001*	<0.001*
8mm	--	--	NA	<0.001*
activation volume				
group mean	*4340.8±1023.6*	*8129.1±2093.1*	*9134.3±2442.8*	*10089.7±2754*
0mm	NA	0.005*	.006*	0.007*
6mm	--	NA	0.017*	0.018*
8mm	--	--	NA	0.035*
maxima t-value	**4mm isovoxels**			
	0mm	6mm	8mm	10mm
group mean	*12.09±x*	*11.57±x*	*10.61±x*	*9.98±x*
0mm	NA	0.366	0.005*	0.001*
6mm	--	NA	0.002*	<0.001*
8mm	--	--	NA	<0.001*
contrast magnitude				
group mean	*2.54±0.21*	*1.70±0.19*	*1.38±0.20*	*1.20±0.20*
0mm	NA	0.006*	0.001*	<0.001*
6mm	--	NA	0.031*	<0.001*
8mm	--	--	NA	0.237
threshold t-value				
group mean	*4.03±0.01*	*3.89±0.02*	*3.70±0.05*	*3.64±0.02*
0mm	NA	<0.001*	<0.001*	<0.001*
6mm	--	NA	0.002*	<0.001*
8mm	--	--	NA	0.271
activation volume				
group mean	*4553.8±1061.1*	*8861.5±2197.5*	*9777.2±2541.7*	*10510.8±2839*
0mm	NA	0.004*	0.006*	0.008*
6mm	--	NA	0.034*	0.031*
8mm	--	--	NA	0.045*

* $p<0.05$ in a paired t-test.

Table 4. Smoothing kernel effects on SMC activation during sequence learning.

maxima t-value	**3mm isovoxels**			
	0mm	6mm	8mm	10mm
group mean†	*11.72±0.55*	*10.44±0.77*	*9.78±0.79*	*8.63±0.68*
0mm	NA	0.055	0.012*	<0.001*
6mm	--	NA	0.067	<0.001*
8mm	--	--	NA	0.001*
contrast magnitude				
group mean	*3.91±0.45*	*1.84±0.24*	*1.43±0.15*	*1.37±0.19*
0mm	NA	<0.001*	<0.001*	<0.001*
6mm	--	NA	0.075	0.014*
8mm	--	--	NA	0.630
threshold t-value				
group mean	*4.24±0.01*	*4.01±0.02*	*3.87±0.02*	*3.78±0.02*
0mm	NA	<0.001*	<0.001*	<0.001*
6mm	--	NA	<0.001*	<0.001*
8mm	--	--	NA	<0.001*
activation volume				
group mean	*4932.7±983.7*	*9936.0±2070.7*	*11576.8±2354*	*13001.5±2607*
0mm	NA	0.001*	<0.001*	0.001*
6mm	--	NA	<0.001*	<0.001*
8mm	--	--	NA	<0.001*
maxima t-value	**4mm isovoxels**			
	0mm	6mm	8mm	10mm
group mean	*10.81±0.39*	*9.93±0.71*	*9.37±0.72*	*9.1±0.71*
0mm	NA	0.133	0.021*	0.009*
6mm	--	NA	0.002*	0.027*
8mm	--	--	NA	0.430
contrast magnitude				
group mean	*4.06±0.51*	*2.01±0.40*	*1.74±0.36*	*1.20±0.15*
0mm	NA	<0.001*	<0.001*	<0.001*
6mm	--	NA	0.104	0.074
8mm	--	--	NA	0.138
threshold t-value				
group mean	*4.03±0.01*	*3.89 ±0.02*	*3.75±0.02*	*3.64±0.02*
0mm	NA	<0.001*	<0.001*	<0.001*
6mm	--	NA	<0.001*	<0.001*
8mm	--	--	NA	<0.001*
activation volume		+		
group mean	*5568.0±1008.0*	*10545.2±2046*	*11904.0±2361*	*13533.5±2855*
0mm	NA	0.001*	<0.001*	0.002*
6mm	--	NA	0.001*	0.006*
8mm	--	--	NA	0.021*

* $p<0.05$ in a paired t-test.

Table 5. Smoothing kernel effects on hippocampal connectivity with SMC hand representation.

Repetitive tapping	**Smooth 6**				**Smooth 10**			
Structural	coordinates	t-value	extent	volume	coordinates	t-value	extent	volume
A1^{-}	(38,-24,46)	4.23	4	256	(34,-24,46)	4.06	30	1920
A2^{-}	(38,-24,46)	5.43	46	2944	(38,-16,54)	4.58	54	3456
A3^{-}	(38,-24,46)	5.15	45	2880	(30,-16,62)	4.79	54	3456
B1^{-}	(38,-24,46)	4.52	14	896	(38,-24,46)	4.44	44	2816
B2^{-}	(38,-24,46)	4.51	14	896	(38,-24,46)	4.39	43	2752
B3^{-}	(38,-24,46)	4.57	16	1024	(38,-24,46)	4.15	43	2752
C1^{-}	(38,-24,46)	4.52	10	640	(38,-24,46)	4.41	42	2688
C2^{-}	--	--	--	--	(34,-24,46)	3.55	3	192
C3^{-}	--	--	--	--	(34,-24,46)	3.50	4	256
Functional tapseed^{-}	(42,-24,58)	7.23	54	3456	(30,-16,62)	5.96	54	3456
Sequence learning								
Structural	coordinates	t-value	extent	volume	coordinates	t-value	extent	volume
A1^{-} (post)	(-42,-28,58)	5.12	35	2240	(-38,-32,46)	4.76	43	2752
(pre)	(-38,-12,62)	5.00	7	448	(-38,-12,62)	4.82	21	1344
A2^{-} (post)	(-34,-36,50)	5.06	30	1920	(-34,-36,50)	4.45	38	2432
(pre)	(-34,-12,66)	4.67	8	512	(-34,-12,66)	4.20	8	512
A3^{-} (post)	(-38,-28,46)	5.17	31	1984	(-38,-28,46)	4.20	32	2048
(pre)	(-38,-12,62)	4.20	5	320	(-34,-12,66)	3.91	6	384
B1^{-} (post)	(-38,-32,46)	5.37	30	1920	(-38,-32,46)	5.02	39	2496
(pre)	(-34,-12,66)	5.83	8	512	(-34,-12,66)	5.61	11	704
B2^{-} (post)	(-42,-32,50)	4.78	31	1984	(-38,-32,46)	4.33	38	2432
(pre)	(-34,-12,66)	4.67	8	512	(-34,-12,66)	4.88	10	640
B3^{-}	--	--	--	--	--	--	--	--
C1^{-} (post)	(-38,-32,46)	5.48	26	1664	(-38,-32,46)	5.33	40	2560
(pre)	(-38,-16,62)	4.42	9	576	(-34,-12,66)	5.76	21	1344
C2^{-} (post)	(-38,-32,46)	3.84	6	384	(-38,-32,46)	3.78	18	1152
(pre)	--	--	--	--	(-38,-12,62)	3.69	5	320
C3^{-}	--	--	--	--	--	--	--	--
Functional memseed^{-} (post)	(-34,-36,54)	5.46	41	2624	(-34,-36,50)	7.67	42	2688
(pre)	(-38,-12,62)	4.98	25	1600	(-34,-12,66)	7.24	45	2880
memseed^{+} (pre)	(34,-24,58)	3.98	5	320	(34,-24,58)	4.00	27	1728

Table 6. Hippocampal connectivity with SMC hand representation from single voxels.

	Repetitive tapping				Sequence learning			
M-L plane[1]	coordinates	area	t-value	extent	coordinates	area	t-value	extent
Medial	(34,-16,62)	pre	4.41	31	(-34,-12,66)	pre	4.39	8
	(42,-24,46)	post	4.23	14	(-46,-28,58)	post	4.07	33
Central	(34,-16,62)	pre	3.64	28	(-34,-12,66)	pre	4.50	9
	(38,-24,46)	post	3.94	11	(-38,-32,50)	post	3.95	30
Lateral	(34,-28,54)	pre	3.63	13	(-38,-12,62)	pre	3.71	3
	(38,-24,46)	post	3.84	7	(-42,-28,58)	post	3.49	17
A-P plane[2]								
Anterior	(42,-12,50)	pre	3.87	19	(-38,-12,62)	pre	4.25	7
	(34,-24,46)	post	3.98	5	(-46,-28,58)	post	4.28	37
Middle	(34,-16,54)	pre	3.84	29	(-34,-12,66)	pre	4.81	7
	(38,-24,46)	post	4.29	12	(-46,-28,58)	post	4.08	28
Posterior	(34,-16,54)	pre	3.85	24	(-34,-12,66)	pre	5.85	21
	(42,-24,46)	post	4.27	17	(-38,-32,46)	post	6.19	41

[1]Voxels sampled from the M-L plane consisted of alternate voxels in the central third of the hippocampus, one voxel each from the B1, B2, and B3 structural seeds.

[2]Voxels sampled in the A-P plane consisted of every third voxel in the medial third of the hippocampus, one voxel each from the A1, B1, and C1 structural seeds.

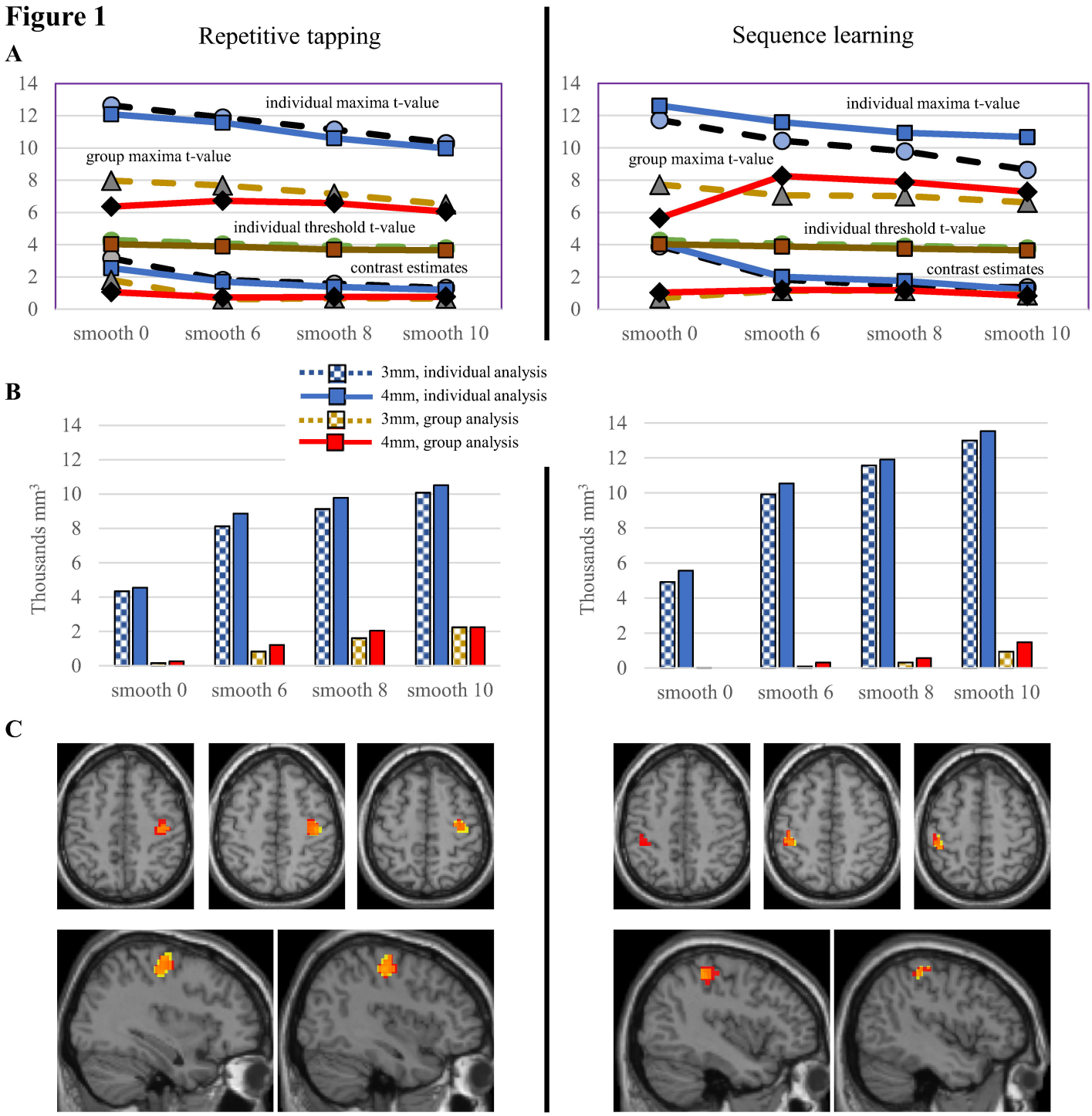

Fig 1. Effects of smoothing kernel and voxel size on SMC individual and group activation during motor tasks. (A) The threshold and parameters from activation maxima are plotted with no smoothing ("smooth 0") and three Gaussian smoothing kernels (6, 8, and 10mm FWHM), each applied to 3- and 4-mm isovoxels (solid and dashed lines, respectively). Activation parameter differences related to voxel size were seen in both individual and group analyses during repetitive tapping and sequence learning; increases in smoothing kernel above 6mm produced small decreases in threshold, contrast magnitude, and maximal t-value. Group analyses yielded lower values than individual analyses. (B) Despite decreases in parameter values, larger smoothing kernels produced larger activation volumes, both within (blue) and between individuals (gold and red). (C) With a smoothing kernel of 10mm, group analysis yielded overlapping volumes of activation for 3mm (yellow) and 4mm isovoxels (red), with a slightly larger activation cluster for 4mm isovoxels during sequence learning.

Figure 2

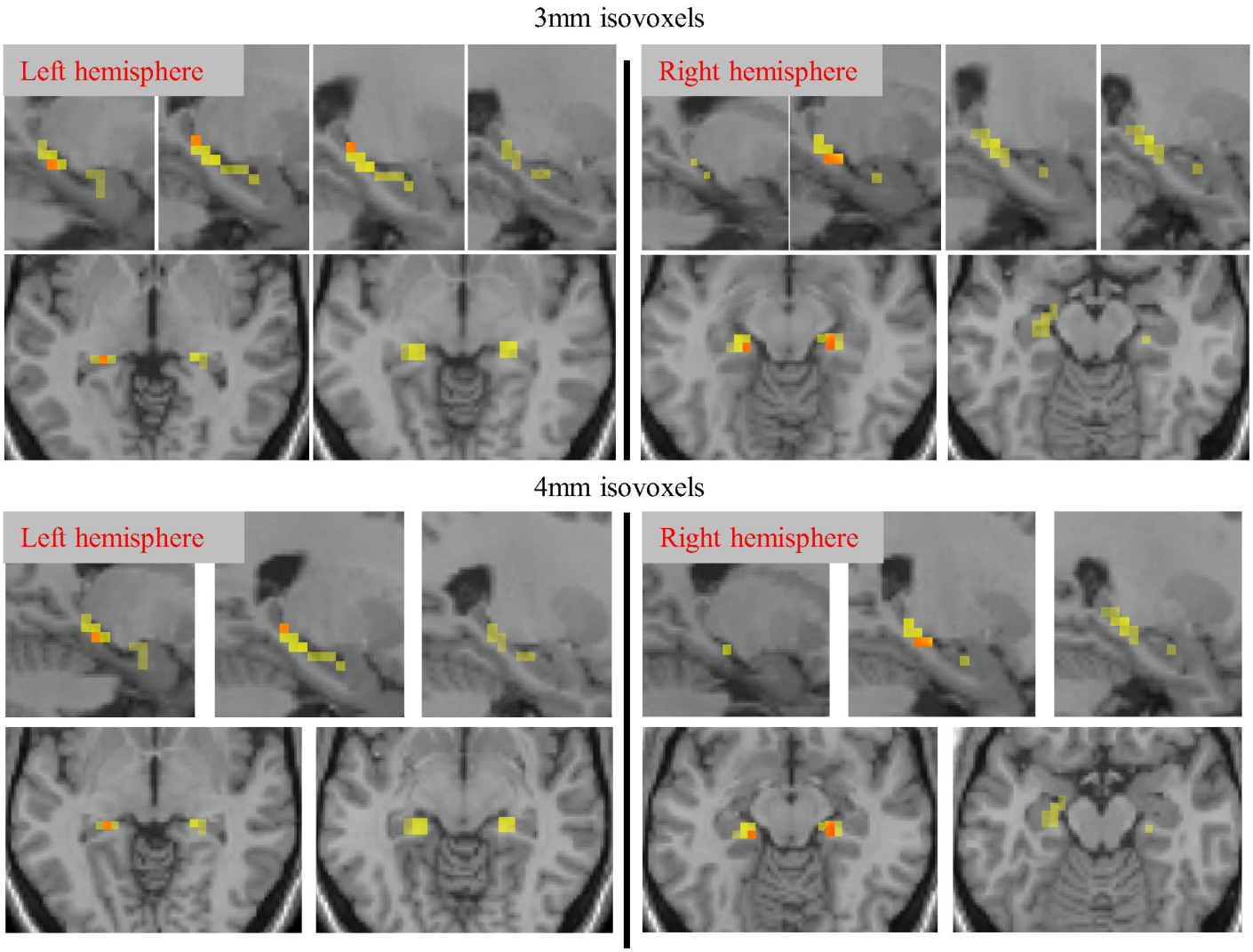

Fig 2. Hippocampal activation during repetitive tapping detected by comparing signal with different smoothing kernels. Both for 3mm and 4mm isovoxels, greater activation was observed in the medial/central hippocampus with the 10mm vs. 6mm smoothing kernel. Analysis was restricted to the hippocampus; red represents more intense activation ($p<0.05$ with FWE correction for intensity), while yellow represents less intense activation over a significant area ($p<0.001$ with FWE correction for extent after $p<0.05$ uncorrected for intensity).

Figure 3

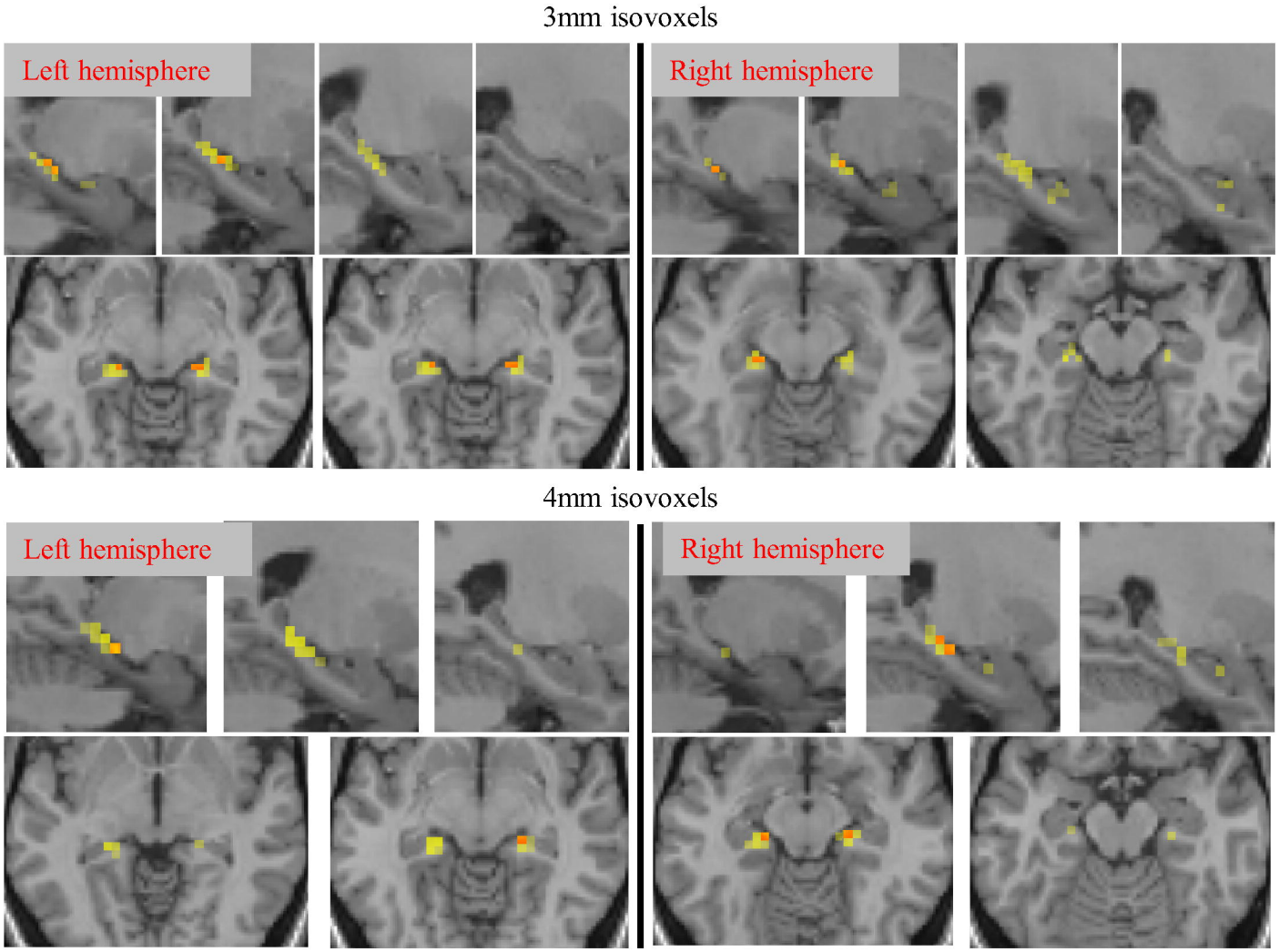

Fig 3. Hippocampal activation during sequence learning detected by comparing signal with different smoothing kernels. Using the same approach as in Fig 2, significantly greater activation was observed in the medial/central hippocampus during sequence learning with the 10mm smoothing kernel, both in the 3mm and 4mm isovoxel analysis.

Figure 4

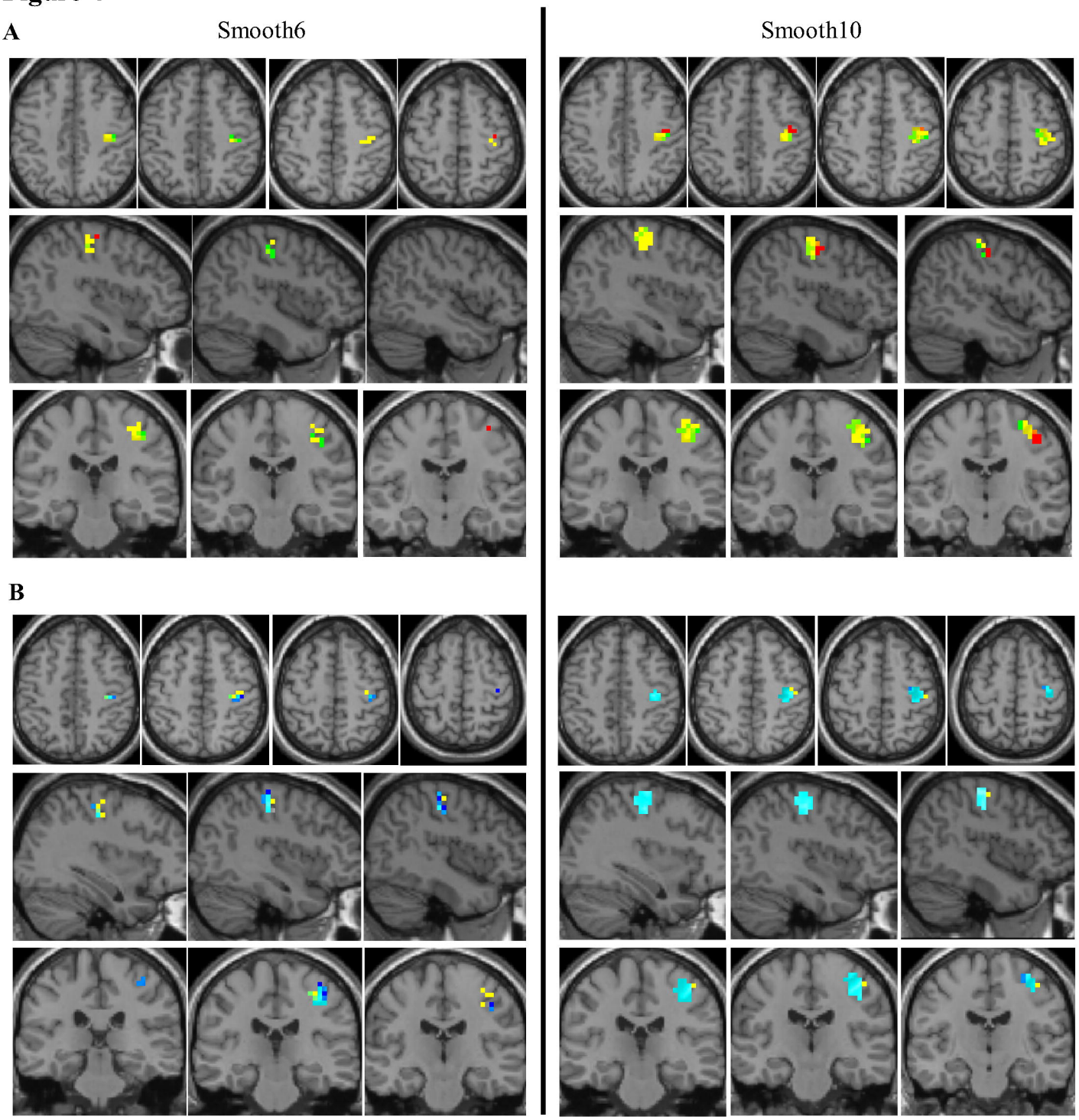

Fig 4. Hippocampal connectivity from structural seeds during repetitive tapping. (A) Random effects group connectivity with the SMC hand representation was plotted from medial structural seeds along the longitudinal axis of the hippocampus, including seeds A1 (red, anterior-medial), B1 (yellow, central-medial), and C1 (green, posterior-medial). A larger area of connectivity was observed with 10mm smoothing, prominent in precentral gyrus; connectivity from the anterior seed A1 was anterolateral, with distinct areas of connectivity from B1 and C1. (B) Connectivity plotted from structural seeds along the medial/lateral axis of the hippocampus, including seeds B1 (yellow, central-medial), B2 (cyan, central-middle), and B3 (dark blue, central-lateral). A larger area of connectivity was observed with 10mm smoothing, where topography was obscured due to extensive, overlapping connectivity from B2. Connectivity was clearly topographical with 6mm smoothing, extending further posterior from lateral seeds.

Figure 5

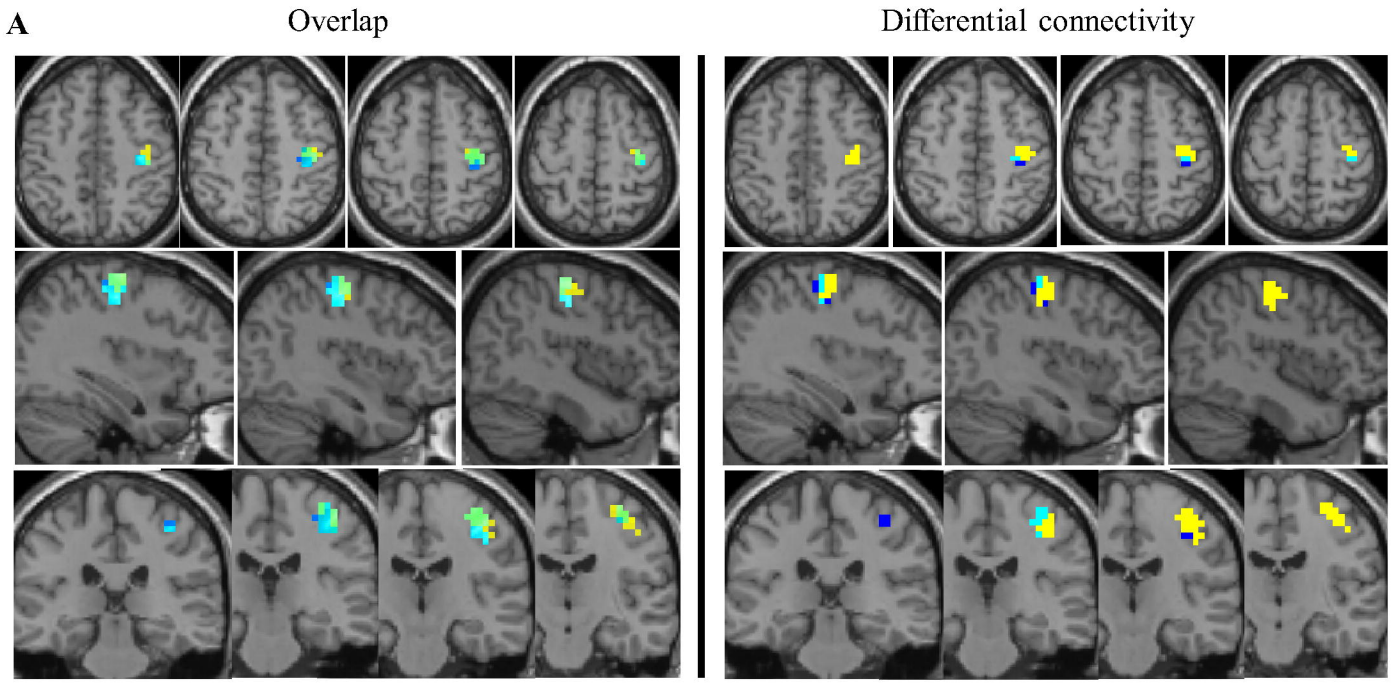

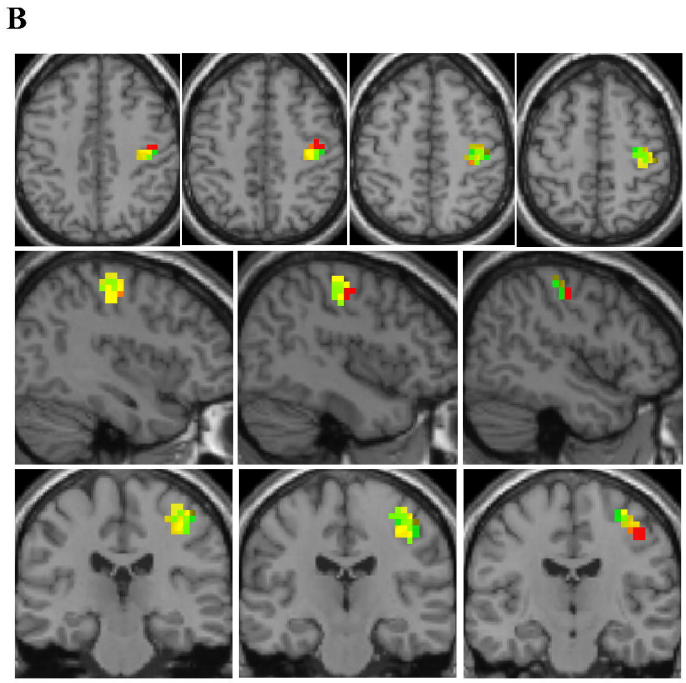

Fig 5. Topography in SMC connectivity maps from individual hippocampal voxels. (A) Connectivity maps from three central voxels in the medial-lateral plane; overlapping connectivity from adjacent voxels is shown on the left, whereas differential connectivity is shown on the right (lateral > middle is dark blue, middle > medial is cyan, medial is yellow). (B) Connectivity maps from three medial voxels along the longitudinal plane; anterior seed is red, middle is yellow, and posterior is green.

Figure 6

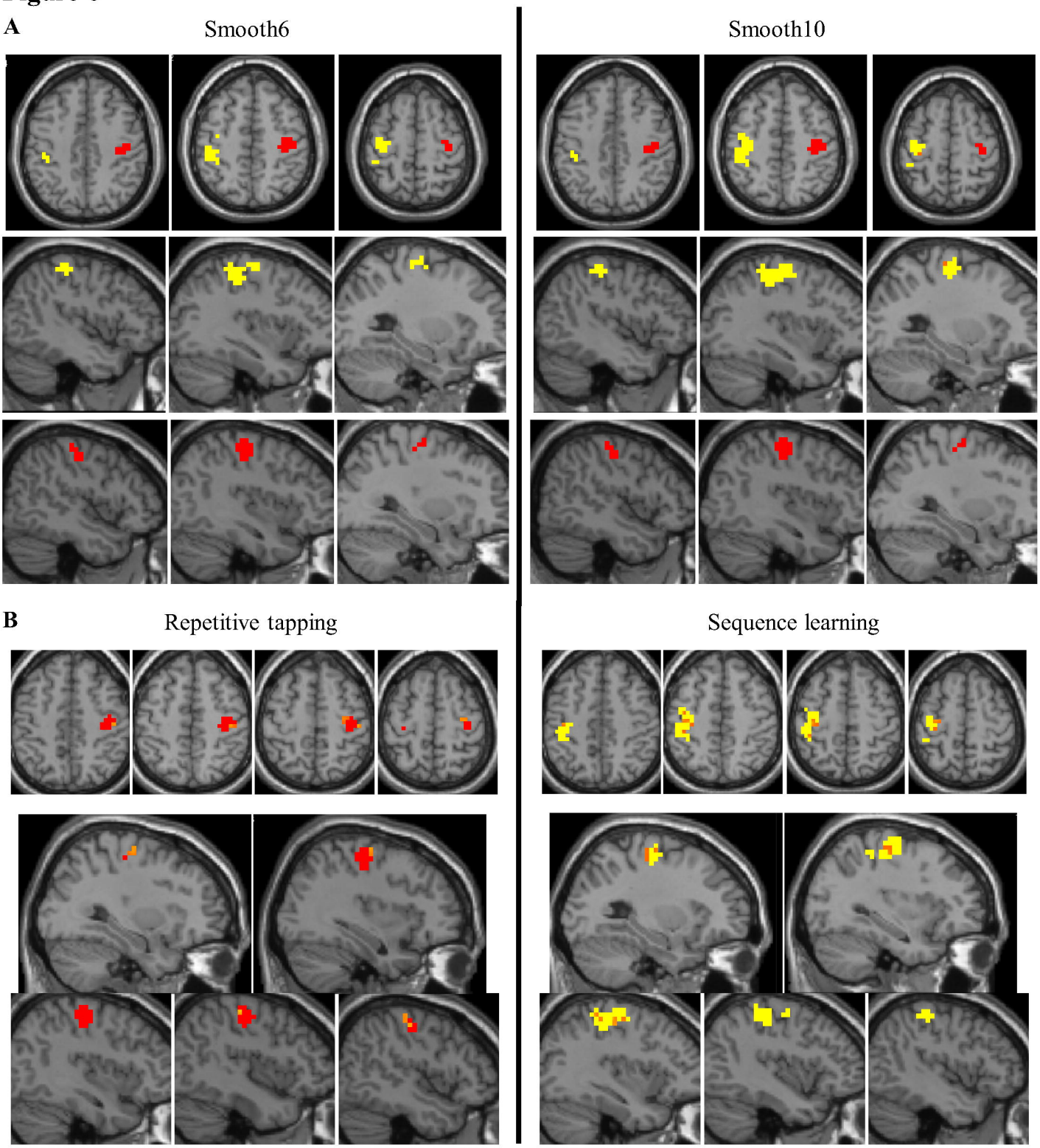

Fig 6. Hippocampal-SMC connectivity from functional seeds. (A) Connectivity from tapseed⁻ during repetitive tapping (red) and tapmem⁻ during sequence learning (yellow) were similar in location and extent for 6mm and 10mm smoothing kernels. (B) Hippocampal voxels with smoothing-dependent motor activity showed significant connectivity within the hand representation, overlapping connectivity from functional seeds (overlap in orange).